Vector lattice Boltzmann equations: from magnetohydrodynamics to active matter

Paul J. Dellar

To appear in *Progress in Industrial Mathematics at ECMI 2021* ed. M. Ehrhardt *et al*, The European Consortium for Mathematics in Industry, Springer 2022.

Abstract We present a lattice Boltzmann algorithm for simulating magnetohydrodynamics, and extend it to simulate the Jeffery equation that describes the rotating orientations of axisymmetric particles in a dilute suspension. Both systems involve material vector fields that evolve through the curl of another vector field. Both systems thus require an underlying kinetic formulation using vector fields, in contrast to the scalar fields used in the Boltzmann equation, and in lattice Boltzmann algorithms for hydrodynamics. Simulating Jeffery's equation requires extra gradient terms that cannot be written in conservation form. These gradients are obtained locally at grid points using the non-equilibrium parts of the kinetic vector fields representing the particle orientations, and the kinetic scalar fields representing the suspending fluid. The kinetic formulation is discretised using a Strang splitting between advection to neighbouring grid points and local algebraic operations at grid points.

1 Introduction

Magnetohydrodynamics (MHD) describes the flow of electrically conducting fluids in magnetic fields by coupling the Maxwell and Navier–Stokes equations. MHD flows arise in the interiors of stars and planets, in smelting and processing liquid metals and semiconductors, and in magnetic confinement fusion reactors [5]. The MHD equations have many structural similarities with recently-developed continuum models for suspensions of rod-like particles [13, 22, 23] that are based on Jeffery's equation for a single axisymmetric particle in Stokes flow [2, 16, 17]. This chapter describes how a numerical method for solving the MHD equations [6] using the lattice Boltzmann approach [1, 19] can be adapted to simulate these suspensions.

Paul J. Dellar
Oxford Centre for Industrial and Applied Mathematics, Mathematical Institute, University of Oxford, Radcliffe Observatory Quarter, Oxford OX2 6GG, UK, e-mail: dellar@maths.ox.ac.uk

2 Lattice Boltzmann hydrodynamics

The Boltzmann equation describes a rarefied gas using a single scalar field $f(\mathbf{x},\mathbf{c},t)$ for the number density of particles at position $\mathbf{x}$ moving with velocity $\mathbf{c}$ at time t,

$$\partial_t f + \mathbf{c}\cdot\nabla f = C[f,f]. \tag{1}$$

The left-hand side represents linear advection of f with the particle velocity $\mathbf{c}$. All nonlinearity is confined to the right-hand side. Boltzmann's binary collision operator $C[f,f]$ describes collisions between pairs of particles via a nonlocal integral operator over $\mathbf{c}$. The Navier–Stokes equations describe solutions of the Boltzmann equation that vary slowly compared to the timescale of collisions [4].

The lattice Boltzmann approach restricts $\mathbf{c}$ to a discrete set $\mathbf{c}_0,\ldots,\mathbf{c}_N$, thus replacing $f(\mathbf{x},\mathbf{c},t)$ with a discrete set of functions $f_i(\mathbf{x},t)$ that evolve according to

$$\partial_t f_i + \mathbf{c}_i\cdot\nabla f_i = -\frac{1}{\tau}\left(f_i - f_i^{(0)}\right) \tag{2}$$

for $i=0,\ldots,N$. This right-hand side models collisions through a linear relaxation on a prescribed timescale τ towards equilibria $f_i^{(0)}$ that are prescribed functions of the local fluid density ρ and velocity $\mathbf{u}$. These macroscopic quantities are given by moments of the f_i,

$$\rho = \sum_{i=0}^{N} f_i, \quad \rho\,\mathbf{u} = \sum_{i=0}^{N} \mathbf{c}_i f_i. \tag{3}$$

In 2D, the discrete velocities are commonly chosen to be the nine shown in Fig. 1 with [21]

$$f_i^{(0)} = w_i\rho\left\{1 + 3\,\mathbf{u}\cdot\mathbf{c}_i + \frac{9}{2}\left((\mathbf{c}_i\cdot\mathbf{u})^2 - \frac{1}{3}|\mathbf{u}|^2\right)\right\}. \tag{4}$$

The weights are $w_0 = 4/9$, $w_{1,2,3,4} = 1/9$ and $w_{5,6,7,8} = 1/36$. From (2) we can derive the lattice Boltzmann equation for some transformed variables $\overline{f}_i$,

$$\overline{f}_i(\mathbf{x}+\mathbf{c}_i\Delta t, t+\Delta t) = \overline{f}_i(\mathbf{x},t) - \frac{\Delta t}{\tau+\Delta t/2}\left(\overline{f}_i(\mathbf{x},t) - f_i^{(0)}(\mathbf{x},t)\right). \tag{5}$$

We can integrate (2) along its characteristics [14] for a time step Δt, or we can apply a Strang splitting into advective and algebraic parts that are solved separately [8].

Using a multiple-scales expansion of both the f_i and the time derivative in a small parameter $\varepsilon = \tau/T$ with suitable solvability conditions, we can find solutions of (2) for which ρ and $\mathbf{u}$ evolve on a slow hydrodynamic timescale T according to

$$\partial_t\rho + \nabla\cdot(\rho\mathbf{u}) = 0, \quad \partial_t(\rho\mathbf{u}) + \nabla\cdot(\boldsymbol{\Pi}^{(0)} + \boldsymbol{\Pi}^{(1)} + \cdots) = 0. \tag{6}$$

These are macroscopic mass and momentum conservation laws. The solvability conditions leave ρ and $\mathbf{u}$, the quantities conserved under collisions, unexpanded, while the momentum flux $\boldsymbol{\Pi} = \sum_i \mathbf{c}_i\mathbf{c}_i f_i$ is expanded in ε as $\boldsymbol{\Pi} = \boldsymbol{\Pi}^{(0)} + \boldsymbol{\Pi}^{(1)} + \cdots$.

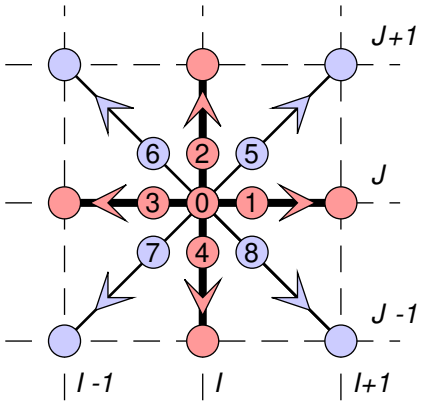

Fig. 1 The nine discrete velocities $\mathbf{c}_0,\ldots,\mathbf{c}_8$ used for the hydrodynamic scalar fields f_i and the five discrete velocities (red, thicker lines) used for the magnetic vector fields $\mathbf{g}_i$. The $\mathbf{c}_i$ are scaled so that each particle propagates from a grid point $\mathbf{x}$ to an adjacent grid point $\mathbf{x}+\mathbf{c}_i\Delta t$ over a time step. The grid points are indexed by I and J.

The equilibria (4) give $\mathbf{\Pi}^{(0)} = c_\mathrm{s}^2\rho\,\mathsf{I} + \rho\,\mathbf{u}\mathbf{u}$ with pressure $p = c_\mathrm{s}^2\rho$ and constant sound speed $c_\mathrm{s} = 1/\sqrt{3}$ in "lattice units" with $\Delta x = \Delta t = 1$. We thus recover the compressible Euler equations at leading order. The multiple-scales expansion gives

$$\mathbf{\Pi}^{(1)} = -\,\tau\rho c_\mathrm{s}^2\left((\nabla\mathbf{u}) + (\nabla\mathbf{u})^\mathsf{T}\right) + \tau\nabla\cdot(\rho\mathbf{u}\mathbf{u}\mathbf{u}), \tag{7}$$

so at next order we recover the Navier–Stokes viscous stress with dynamic viscosity $\mu = \tau\rho c_\mathrm{s}^2$, and an error term $\tau\nabla\cdot(\rho\mathbf{u}\mathbf{u}\mathbf{u})$. The error term is smaller than the viscous stress by the square of the Mach number $|\mathbf{u}|/c_\mathrm{s}$. It is an artifact created by using the discrete velocity set in Fig. 1 with only nine velocities.

3 Lattice Boltzmann magnetohydrodynamics

The magnetic field $\mathbf{B}$ evolves according to Maxwell's equation $\partial_t\mathbf{B} + \nabla\times\mathbf{E} = 0$, where $\mathbf{E}$ is the electric field. We can rewrite this equation in divergence form as

$$\partial_t\mathbf{B} + \nabla\cdot\mathbf{\Lambda} = 0 \tag{8}$$

using the tensor $\mathbf{\Lambda}$ with components $\Lambda_{\alpha\beta} = -\varepsilon_{\alpha\beta\gamma}E_\gamma$. This now resembles the momentum equation in (6), except $\mathbf{\Pi} = \sum_i \mathbf{c}_i\mathbf{c}_i f_i$ is symmetric by construction, while $\mathbf{\Lambda}$ is antisymmetric. It is thus impossible to represent (8) using a set of scalar fields f_i.

Instead, inspired by work conducted at the Schlumberger–Doll laboratory to simulate magnetic resonance imaging of flow in porous media [12], we can represent the magnetic field as the sum of a set of kinetic vector fields $\mathbf{g}_i(\mathbf{x},t)$ that evolve as

$$\partial_t\mathbf{g}_i + \mathbf{c}_i\cdot\nabla\mathbf{g}_i = -\frac{1}{\tau_{\mathbf{\Lambda}}}\left(\mathbf{g}_i - \mathbf{g}_i^{(0)}\right), \tag{9}$$

where

$$\mathbf{g}_i^{(0)} = W_i\left(\mathbf{B} + \Theta^{-1}\mathbf{c}_i\cdot\mathbf{\Lambda}^{(0)}\right), \tag{10}$$

with $\mathbf{\Lambda}^{(0)} = \mathbf{u}\mathbf{B} - \mathbf{B}\mathbf{u}$. It is sufficient to use five discrete velocities in 2D, as shown in Fig. 1, with weights $W_0 = 1/3$, $W_{1,2,3,4} = 1/6$ and lattice constant $\Theta = 1/3$.

Summing (9) over i and applying another multiple-scales expansion gives

$$\partial_t\mathbf{B} + \nabla\cdot\left(\mathbf{\Lambda}^{(0)} + \mathbf{\Lambda}^{(1)} + \cdots\right) = 0, \tag{11}$$

for the moments

$$\mathbf{B} = \sum_{i=0}^{4}\mathbf{g}_i, \quad \mathbf{\Lambda}^{(n)} = \sum_{i=0}^{4}\mathbf{c}_i\,\mathbf{g}_i^{(n)}. \tag{12}$$

We obtain ideal MHD at leading order as $\mathbf{\Lambda}^{(0)} = \mathbf{u}\mathbf{B} - \mathbf{B}\mathbf{u}$. The first correction is

$$\mathbf{\Lambda}^{(1)} = -\tau_{\mathbf{\Lambda}}\,\Theta\,\nabla\mathbf{B}, \tag{13}$$

for which (11) gives the resistive MHD induction equation with resistivity $\eta = \tau_{\mathbf{\Lambda}}\Theta$,

$$\partial_t\mathbf{B} = \nabla\times(\mathbf{u}\times\mathbf{B}) + \eta\nabla^2\mathbf{B}, \tag{14}$$

using $\nabla\cdot\mathbf{B} = 0$. The Lorentz force $(\nabla\times\mathbf{B})\times\mathbf{B}$ exerted by the magnetic field on the fluid can be rewritten as the divergence of the Maxwell stress. The Maxwell stress can be included in the equilibrium momentum flux $\mathbf{\Pi}^{(0)}$ by redefining the $f_i^{(0)}$ [6]. The resulting algorithm has been employed for large simulations of 3D MHD turbulence [24] and to simulate liquid metal cooling blankets for fusion reactors [20].

4 Jeffery's equation for axisymmetric particles

Jeffery's equation describes a torque-free axisymmetric rigid particle immersed in a Stokes flow with a uniform velocity gradient L at infinity [2, 16, 17]. The unit vector $\mathbf{p}$ directed along the symmetry axis evolves according to

$$\dot{\mathbf{p}} = \mathbf{\Omega}\cdot\mathbf{p} + \beta\left(\mathsf{E}\cdot\mathbf{p} - \mathbf{p}\,\mathbf{p}\cdot\mathsf{E}\cdot\mathbf{p}\right), \tag{15}$$

where $\mathbf{\Omega} = \frac{1}{2}(\mathsf{L} - \mathsf{L}^\mathsf{T})$ and $\mathsf{E} = \frac{1}{2}(\mathsf{L} + \mathsf{L}^\mathsf{T})$ are the antisymmetric and symmetric parts of the tensor L. The last term in (15) preserves the normalisation $|\mathbf{p}| = 1$, as $\dot{\mathbf{p}}\cdot\mathbf{p} = 0$. The Bretherton shape parameter β equals $(r^2-1)/(r^2+1)$ for spheroids with aspect ratio r, so $\beta \approx 1$ for slender rods with $r \gg 1$, while $\beta = 0$ for spheres.

To describe a dilute suspension of particles we treat $\mathbf{p}(\mathbf{x},t)$ as a vector field, and replace L with the local velocity gradient $\nabla\mathbf{u}$, assumed to vary on lengthscales much larger than the particle size. We also replace $\dot{\mathbf{p}}$ with a material time derivative,

$$\partial_t\mathbf{p} + \mathbf{u}\cdot\nabla\mathbf{p} = \mathbf{p}\cdot\nabla\mathbf{u} + (\beta-1)\,\mathsf{E}\cdot\mathbf{p} - \beta\,\mathbf{p}\,\mathbf{p}\cdot\mathsf{E}\cdot\mathbf{p}. \tag{16}$$

To make a closer connection with the MHD induction equation, and because lattice Boltzmann algorithms simulate compressible fluids with finite sound speeds, we introduce $\mathbf{P} = \rho\,\mathbf{p}$, normalised by $|\mathbf{P}| = \rho$. The vector field $\mathbf{P}$ evolves according to

$$\partial_t \mathbf{P} = \nabla\times(\mathbf{u}\times\mathbf{P}) - \mathbf{u}\nabla\cdot\mathbf{P} + (\beta-1)\,\mathbf{E}\cdot\mathbf{P} - (\beta/\rho^2)\,\mathbf{P}\mathbf{P}\cdot\mathbf{E}\cdot\mathbf{P}. \tag{17}$$

The first term on the right-hand side now exactly matches the MHD induction equation (14). The remaining terms arise because we have replaced $\nabla\cdot\mathbf{B}=0$ by $|\mathbf{P}|=\rho$, and because particles with $\beta<1$ do not align perfectly with the velocity gradient, in constrast to magnetic fields. However, if we represent $\mathbf{P}=\sum_i \mathbf{g}_i$ as in Sect. 3 we can obtain $\nabla\cdot\mathbf{P}$ from $\mathrm{Tr}\,\mathbf{\Lambda}$ using (13), and $\mathbf{E}$ from $\mathbf{T}=\mathbf{\Pi}-\mathbf{\Pi}^{(0)}$ using (7), giving

$$\partial_t \mathbf{P} = \nabla\times(\mathbf{u}\times\mathbf{P}) + \frac{1}{\tau_{\mathbf{\Lambda}}\Theta}\,\mathbf{u}\,\mathrm{Tr}\,\mathbf{\Lambda} + \frac{1-\beta}{2\tau c_\mathrm{s}^2\rho}\,\mathbf{P}\cdot\mathbf{T} + \frac{\beta}{2\tau c_\mathrm{s}^2\rho^3}\,\mathbf{P}\mathbf{P}\cdot\mathbf{T}\cdot\mathbf{P}. \tag{18}$$

5 Discretisation by Strang splitting

To discretise the above, we separate the algebraic right-hand side of the kinetic equation for the $\mathbf{g}_i$ from the pure advection $\partial_t\mathbf{g}_i+\mathbf{c}_i\cdot\nabla\mathbf{g}_i=0$ that gives rise to the $\nabla\times(\mathbf{u}\times\mathbf{P})$ term. The advection can be solved exactly, as in (5), and the algebraic terms by the Crank–Nicolson method. The lattice Boltzmann method relies upon an almost exact cancellation between the Crank–Nicolson truncation error and the error due to Strang splitting [3, 8].

The algebraic terms are best treated by evolving the moments of the $\mathbf{g}_i$, then reconstructing the $\mathbf{g}_i$ from the moments. For example, if we represent $\mathbf{P}$ using the five discrete velocities shown in Fig. 1, $\mathbf{P}$, $\mathbf{\Lambda}$ and $\mathbf{M}=\sum_i \mathbf{c}_i\mathbf{c}_i\mathbf{g}_i$ form a basis of moments since $M_{\alpha\beta\gamma}\equiv 0$ for $\alpha\neq\beta$. We can reconstruct the $\mathbf{g}_i$ from

$$g_{i\beta} = \tfrac{1}{2}\left(\xi_{i\alpha}\Lambda_{\alpha\beta} + \xi_{i\gamma}\xi_{i\alpha}M_{\gamma\alpha\beta}\right) \text{ for } i\neq 0, \quad g_{0\beta} = P_\beta - M_{\alpha\alpha\beta}. \tag{19}$$

We can similarly complete ρ, $\rho\mathbf{u}$, $\mathbf{\Pi}$ to form a basis for the nine moments of the f_i.

The non-equilibrium momentum flux $\mathbf{T}=\mathbf{\Pi}-\mathbf{\Pi}^{(0)}$ evolves under collisions as

$$\partial_t \mathbf{T} = -(1/\tau)\mathbf{T}. \tag{20}$$

Discretising this ODE using the Crank–Nicolson method gives

$$\frac{\mathbf{T}(t+\Delta t)-\mathbf{T}(t)}{\Delta t} = -\frac{1}{2\tau}\left(\mathbf{T}(t+\Delta t)+\mathbf{T}(t)\right), \tag{21}$$

which rearranges into

$$\mathbf{T}' = \frac{\tau-\Delta t/2}{\tau+\Delta t/2}\,\mathbf{T}, \tag{22}$$

on writing $\mathbf{T}'$ for $\mathbf{T}(t+\Delta t)$ and $\mathbf{T}$ for $\mathbf{T}(t)$. Similarly, the Crank–Nicolson method for the evolution of $\mathrm{Tr}\,\mathbf{\Lambda}$, using $\mathrm{Tr}\,\mathbf{\Lambda}^{(0)}=0$, gives

$$\mathrm{Tr}\,\mathbf{\Lambda}' = \frac{\tau_{\mathbf{\Lambda}}-\Delta t/2}{\tau_{\mathbf{\Lambda}}+\Delta t/2}\,\mathrm{Tr}\,\mathbf{\Lambda}. \tag{23}$$

A partial Crank–Nicolson approximation for the algebraic terms in (18) is

$$\frac{\mathbf{P}'-\mathbf{P}}{\Delta t} = \frac{1}{\tau_{\mathbf{\Lambda}}\Theta}\,\mathbf{u}\,\mathrm{Tr}\,\widetilde{\mathbf{\Lambda}} + \frac{1-\beta}{2\tau\rho c_\mathrm{s}^2}\,\mathbf{P}\cdot\widetilde{\mathbf{T}} + \frac{\beta}{2\tau\rho^3 c_\mathrm{s}^2}\,\mathbf{P}\,\mathbf{P}\cdot\widetilde{\mathbf{T}}\cdot\mathbf{P}, \tag{24}$$

where $\widetilde{\mathbf{\Lambda}}=\frac{1}{2}(\mathbf{\Lambda}'+\mathbf{\Lambda})$ and $\widetilde{\mathbf{T}}=\frac{1}{2}(\mathbf{T}'+\mathbf{T})$. The right-hand side is evaluated using only $\mathbf{P}$, rather than a mixture of $\mathbf{P}$ and $\mathbf{P}'$. A justification for this approximation is that $\mathrm{Tr}\,\mathbf{\Lambda}$ and $\mathbf{T}$ evolve on the fast collisional timescales $\tau_{\mathbf{\Lambda}}$ and τ, while $\mathbf{P}$ evolves on a slow hydrodynamic timescale. Solving (24) for $\mathbf{P}'$ using (22) and (23) gives

$$\mathbf{P}' = \mathbf{P} + \frac{1}{\Theta}\,\frac{\Delta t}{\tau_{\mathbf{\Lambda}}+\Delta t/2}\,\mathbf{u}\,\mathrm{Tr}\,\mathbf{\Lambda} + \frac{1-\beta}{2c_\mathrm{s}^2\rho}\,\frac{\Delta t}{\tau+\Delta t/2}\,\mathbf{P}\cdot\mathbf{T} + \frac{\beta}{2c_\mathrm{s}^2\rho^3}\,\frac{\Delta t}{\tau+\Delta t/2}\,\mathbf{P}\,\mathbf{P}\cdot\mathbf{T}\cdot\mathbf{P}, \tag{25}$$

where every quantity on the right-hand side is evaluated at time t.

To evolve the remaining moments $\mathbf{\Lambda}$ and $\mathbf{M}$, we form the non-equilibrium part of each moment using $\mathbf{P}$, evolve the non-equilibrium part using a Crank–Nicolson time step, then reconstruct the full moment using $\mathbf{P}'$, for example

$$\mathbf{\Lambda}' = \mathbf{\Lambda}^{(0)\prime} + \frac{\tau_{\mathbf{\Lambda}}-\Delta t/2}{\tau_{\mathbf{\Lambda}}+\Delta t/2}\left(\mathbf{\Lambda}-\mathbf{\Lambda}^{(0)}\right), \tag{26}$$

where $\mathbf{\Lambda}^{(0)}=\mathbf{u}\mathbf{P}-\mathbf{P}\mathbf{u}$ and $\mathbf{\Lambda}^{(0)\prime}=\mathbf{u}\mathbf{P}'-\mathbf{P}'\mathbf{u}$. This procedure ensures that the relations (7) and (13) expressing $\mathbf{E}$ and $\nabla\cdot\mathbf{P}$ in terms of non-equilibrium moments hold despite $\mathbf{P}$ changing. It is equivalent to the so-called exact difference method for implementing body forces in lattice Boltzmann hydrodynamics [9, 18]. Taking the trace of (26) gives (23) as above, since $\mathrm{Tr}\,\mathbf{\Lambda}^{(0)\prime}=\mathrm{Tr}\,\mathbf{\Lambda}^{(0)}=0$. From $\mathbf{P}'$, $\mathbf{\Lambda}'$ and $\mathbf{M}'$ we can reconstruct the post-collisional functions $\mathbf{g}_i'$ using (19), then advect them to adjacent grid points to obtain the $\mathbf{g}_i$ at the next time step,

$$\mathbf{g}_i(\mathbf{x},t+\Delta t) = \mathbf{g}_i'(\mathbf{x}-\mathbf{c}_i\Delta t). \tag{27}$$

6 Numerical example: Poiseuille flow of a suspension of long rods

Jeffery's equation describes how fluid flow affects the orientation of suspended particles. To obtain interesting behaviour, the particles should in turn affect the flow. Continuum models of active rod suspensions [13, 22, 23] contain a stress proportional to $\mathbf{p}\mathbf{p}$, equivalent to the Maxwell stress due to a magnetic field in an incompressible fluid. As a first step, we consider a suspension of passive long rods ($r\gg 1$) large enough to be unaffected by Brownian motion. The momentum flux is then [10, 11, 15]

$$\mathbf{\Pi} = c_\mathrm{s}^2\rho\,\mathbf{I} + \rho\,\mathbf{u}\mathbf{u} - \mu\left(2\,\mathbf{E} + N\,\mathbf{p}\mathbf{p}\mathbf{p}\cdot\mathbf{E}\cdot\mathbf{p}\right). \tag{28}$$

The anisotropic extra stress along $\mathbf{pp}$ proportional to the non-Newtonian parameter $N \sim \phi r^2/\log r$ can be significant for $r \gg 1$ even at low volume fractions ϕ.

This anisotropic viscous stress is mathematically identical to a common model for the stress in a strongly magnetised plasma, known as Braginskii MHD, if we take $\mathbf{p} = \mathbf{B}/|\mathbf{B}|$ to be a unit vector parallel to the magnetic field. To obtain (28) from our kinetic formulation we adjust (22) to apply a different relaxation time $\tau_\parallel$ to the component $\mathbf{p}\cdot\mathsf{T}\cdot\mathbf{p}$ of the stress [7]

$$\mathsf{T}' = \frac{\tau_\perp - \Delta t/2}{\tau_\perp + \Delta t/2}\,\mathsf{T} + \left(\frac{\tau_\parallel - \Delta t/2}{\tau_\parallel + \Delta t/2} - \frac{\tau_\perp - \Delta t/2}{\tau_\perp + \Delta t/2}\right)\mathbf{ppp}\cdot\mathsf{T}\cdot\mathbf{p}. \tag{29}$$

The time $\tau_\perp$ determines the fluid viscosity perpendicular to (or in the absence of) the particles, while $\tau_\parallel = (1+N/2)\,\tau_\perp$ is enhanced by a factor of $N/2$ as in (28). We can still obtain a kinetic approximation to the strain rate from the isotropic formula

$$\mathsf{E} = \big(\mathsf{T} - \mathsf{T}'\big)/(2\rho\, c_s^2 \Delta t), \tag{30}$$

because E is determined by the advective terms on the left-hand side of (5).

The Poiseuille flow of such a suspension, with $\mathbf{u} = u(y,t)\,\hat{\mathbf{x}}$ driven by a constant body force $f\,\hat{\mathbf{x}}$ in the usual rheological axes, is governed by the coupled system [10]

$$\partial_t\theta = -(1/2)\,(1-\beta\cos 2\theta)\,\partial_y u + \kappa\,\partial_{yy}\theta, \tag{31a}$$
$$\partial_t u = f + \partial_y\,(\nu(\theta)\,\partial_y u). \tag{31b}$$

The effective viscosity is a function of the angle θ between the rods and the x-axis,

$$\nu(\theta) = \nu_0\big(1 + N\sin^2\theta\cos^2\theta\big). \tag{32}$$

This system also includes a small orientational diffusivity $\kappa \propto \tau_\Lambda$ analogous to the resistivity in the MHD induction equation (14). For $\beta < 1$ it has solutions that oscillate in time as the rods rotate. Figure 2 shows this oscillating parabolic Poiseuille profile in a numerical experiment with $\beta = 0.9$, $N = 10$, and $\theta = \sin(2\pi y)$ initially.

7 Conclusion

A lattice Boltzmann approach has been presented for simulating Jeffery's equation that describes the evolution of the orientation field $\mathbf{p}$ for a suspension of axisymmetric rigid particles, exploiting its close similarity with the MHD induction equation. The primary difference is the replacement of the divergence-free constraint $\nabla\cdot\mathbf{B} = 0$ by the normalisation condition $|\mathbf{p}| = 1$. The necessary extra gradient information is available locally at grid points from the non-equilibrium parts of the hydrodynamic and orientational kinetic fields. Jeffery's equation underpins continuum models of many physical systems involving suspensions of non-spherical particles: liquid crystals, active rods, gyrotactic bacteria, and ferromagnetic fluids [22, 23].

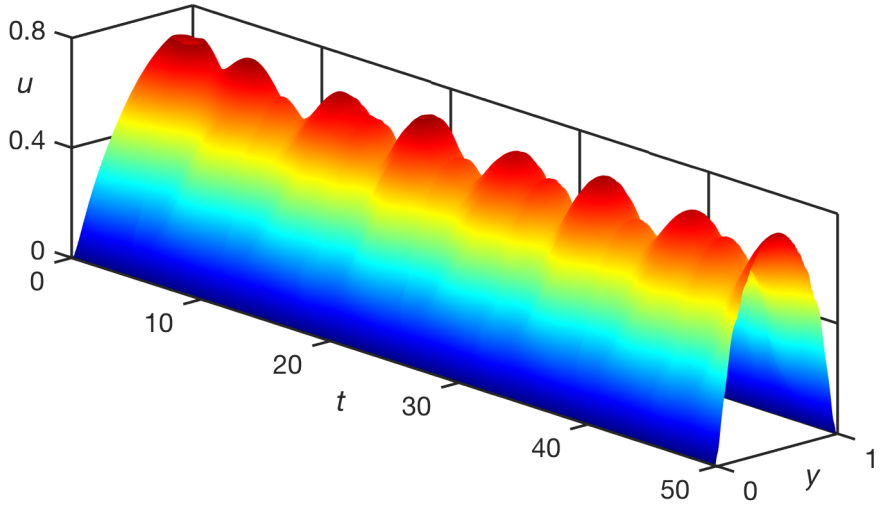

Fig. 2 Oscillatory streamwise velocity in Poiseuille flow for a suspension of elongated particles.

References

1. R. Benzi, S. Succi, M. Vergassola, Phys. Rep. **222**, 145 (1992)
2. F.P. Bretherton, J. Fluid Mech. **14**, 284 (1962)
3. R.A. Brownlee, A.N. Gorban, J. Levesley, Phys. Rev. E **75**, 036711 (2007)
4. C. Cercignani, *The Boltzmann Equation and its Applications* (Springer, New York, 1988)
5. P.A. Davidson, *An Introduction to Magnetohydrodynamics*, 2nd edn. (Cambridge University Press, Cambridge, 2016)
6. P.J. Dellar, J. Comput. Phys. **179**, 95 (2002)
7. P.J. Dellar, Comput. Fluids **46**, 201 (2011)
8. P.J. Dellar, Comput. Math. Applic. **65**, 129 (2013)
9. P.J. Dellar, SIAM J. Sci. Comput. **36**, A2507 (2014)
10. J.G. Evans, in *Theoretical Rheology*, ed. by J.F. Hutton, J.R.A. Pearson, K. Walters (Applied Science Publishers, London, 1975), pp. 224–232
11. H. Giesekus, Rheol. Acta **2**, 50 (1962)
12. R.A. Guyer, K.R. McCall, Phys. Rev. B **62**, 3674 (2000)
13. Y. Hatwalne, S. Ramaswamy, M. Rao, R.A. Simha, Phys. Rev. Lett. **92**, 118101 (2004)
14. X. He, S. Chen, G.D. Doolen, J. Comput. Phys. **146**, 282 (1998)
15. E.J. Hinch, L.G. Leal, J. Fluid Mech. **52**, 683 (1972)
16. G.B. Jeffery, Proc. R. Soc. Lond A **102**, 161 (1922)
17. M. Junk, R. Illner, J. Math. Fluid Mech. **9**, 455 (2007)
18. A.L. Kupershtokh, Comput. Math. Applic. **59**, 2236 (2010)
19. P. Lallemand, L.S. Luo, M. Krafczyk, W.A. Yong, J. Comput. Phys. **431**, 109713 (2021)
20. M. Pattison, K. Premnath, N. Morley, M. Abdou, Fusion Eng. Design **83**, 557 (2008)
21. Y.H. Qian, D. d'Humières, P. Lallemand, Europhys. Lett. **17**, 479 (1992)
22. S. Ramaswamy, Annu. Rev. Condens. Matter Phys. **1**, 323 (2010)
23. D. Saintillan, M.J. Shelley, in *Complex Fluids in Biological Systems: Experiment, Theory, and Computation*, ed. by S.E. Spagnolie (Springer, New York, 2015), pp. 319–355
24. G. Vahala, B. Keating, M. Soe, J. Yepez, L. Vahala, J. Carter, S. Ziegeler, Commun. Comput. Phys. **4**, 624 (2008)